STUDY OF THE DYNAMIC INTERACTION BETWEEN A FAST RUNNING CRACK AND AN INCLUSION USING THE TIME DOMAIN BEM

Y. S. WANG[1], J. LEI[1] & D. GROSS[2]
[1]Institute of Engineering Mechanics, Beijing Jiaotong University, Beijing 100044, China
[2] Institute of Mechanics, Technical University of Darmstadt, Darmstadt 64289, Germany

ABSTRACT

In this paper, a fast running crack in an elastic matrix with an inclusion is studied by using the time domain boundary element method (BEM). The bi-material system is divided into two parts along the interface between the inclusion and the matrix. Each part is linear, elastic, homogeneous and isotropic. For the crack surfaces, the non-hypersingular traction boundary integral equations are applied; while for the interface and external boundaries, traditional displacement boundary integral equations are used. In the numerical solution procedure, square root shape functions are adopted as to describe the proper asymptotic behavior in the vicinity of the crack-tips. The integrations over time are analytically computed via linear or constant temporal interpolation functions. The crack growth is modeled by adding new elements of constant length to the moving crack tip, which is controlled by the fracture criterion based on the maximum circumferential stress. The fracture criterion is evaluated to determine the direction and the speed of the crack advance in each time step. As an example, a rectangular plate with a pre-existing edged crack and a circular inclusion under the action of wedged impact loading is computed in details. The numerical results of the crack growth path, running speed, dynamic stress intensity factors (DSIFs) and dynamic interface tractions are presented for various material combinations and geometries. The effects of the inclusion on the fast crack propagation are discussed.

1 INTRODUCTION

In the process of the manufacture, some different phases, such as voids, flaws or inclusions, will be inevitably occurred in the materials. As well, in order to reinforce a material, a particle-reinforced technique has been applied to industrial practice. It is now well known that the pre-existing flaws/inclusions will do a significant effect on the fracture properties in these materials. To better understand the fracture mechanism, the interaction between the pre-existing cracks and inclusions should deserve investigation. Indeed the problem of crack interaction with an elastic inclusion has been an attractive subject of many previous investigations, and the cases of a crack inside, outside, penetrating or lying on the interface were analyzed [1-5]. However, most of the previous publications were focused on the quasi-static crack growth. In this paper, a fast running crack in an elastic matrix with an inclusion is studied by using the time domain boundary element method (BEM). The dynamic interaction between the inclusion and the crack is examined.

2 PROBLEM FORMULATION

Consider a crack propagating to an inclusion embedded in a matrix with arbitrary configurations in plane strain state, see Fig.1. All component materials are assumed isotropic and linearly elastic. The matrix is surrounded by the external boundary $\Gamma_m = \Gamma_\sigma + \Gamma_u$, the interface Γ_s, the upper and lower crack faces $\Gamma_C^{\pm}$. The inclusion is encircled by its boundary Γ_i which is the same as Γ_s. Γ_σ is the part of external boundary with tractions $\hat{t}_\alpha$ being given, and Γ_u the remaining external boundary with the displacements $\hat{u}_\alpha$ being prescribed. The unit normal vectors of all boundaries are shown in Fig.1.

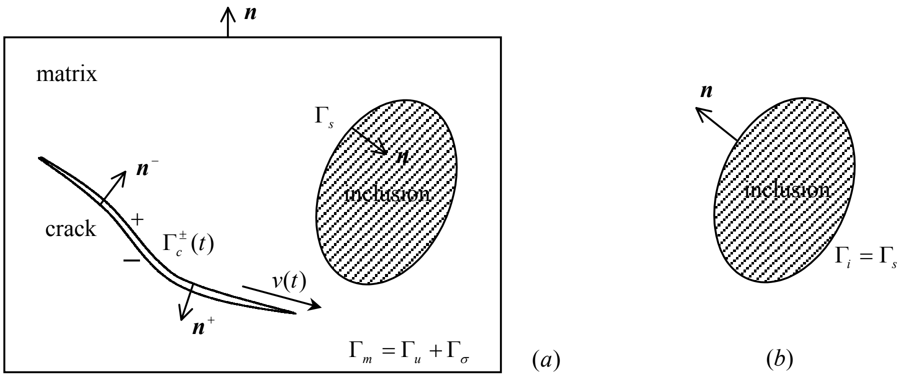

Fig.1 A fast running in an elastic matrix with an elastic inclusion

Nomenclature of some material parameters are shown as follows: Shear modulus μ_j, Lamé constant λ_j, Poisson's ratio ν_j and mass density ρ_j for the matrix (j=1) and inclusion (j=2), respectively. The shear and longitudinal wave velocities are given by $C_T^j = \sqrt{\mu_j / \rho_j}$ and $C_L^j = \sqrt{(\lambda_j + 2\mu_j)/\rho_j}$, respectively.

Assume a general load $\hat{t}_\alpha^c(\boldsymbol{x},t)$ is applied on the crack faces. Then we have

$$t_\alpha(\boldsymbol{x},t) = \sigma_{\alpha\beta}(\boldsymbol{x},t) n_\beta = \hat{t}_\alpha^c(\boldsymbol{x},t), \qquad \boldsymbol{x} \in \Gamma_C^{\pm}(t). \tag{1}$$

If the inclusion and the matrix are perfectly bonded, the interface conditions become

$$t_\alpha^1(\boldsymbol{x},t) = -t_\alpha^2(\boldsymbol{x},t), \;\; u_\alpha^1(\boldsymbol{x},t) = u_\alpha^2(\boldsymbol{x},t), \qquad \boldsymbol{x} \in \Gamma_S \tag{2}$$

which states that forces and displacements are continuous across the interface. At the external boundary, we have

$$t_\alpha(\boldsymbol{x},t) = \hat{t}_\alpha(\boldsymbol{x},t), \qquad \boldsymbol{x} \in \Gamma_\sigma, \tag{3}$$

$$u_\alpha(\boldsymbol{x},t) = \hat{u}_\alpha(\boldsymbol{x},t), \qquad \boldsymbol{x} \in \Gamma_u. \tag{4}$$

In addition, zero initial conditions are assumed, i.e.

$$u_\alpha^j(\boldsymbol{x},t) = \dot{u}_\alpha^j(\boldsymbol{x},t) = 0, \qquad \text{for} \;\; t \le 0. \tag{5}$$

In above equations, $\sigma_{\alpha\beta}^j$ and u_α^j denote the stress and displacement components. The conventional summation rule over double indices is applied with Greek indices $\alpha, \beta, \gamma, \delta = 1,2$ for the present 2D problem.

3 BOUNDARY ELEMENT FORMULATIONS AND NUMERICAL PROCEDURE

As in Ref. [6], we apply two systems of BIEs for different boundaries. At the external boundaries including the interfaces, the traditional time-domain displacement BIEs derived from Betti-

Rayleigh reciprocal theorem are used, while at the crack faces, the non-hypersingular time-domain traction BIEs developed by Zhang et al [7] are employed. Here, we directly list them as follows:

$$
\begin{aligned}
t_{\alpha}^{\Gamma_C} = {} & C_{\alpha\gamma\upsilon\delta}^{1} n_{\gamma}^{1}(\boldsymbol{x}) \int_{0}^{t} \int_{\Gamma_m} \left\{ \boldsymbol{e}_{\delta\varepsilon} \sigma_{\beta\varepsilon\upsilon}^{1G}(\boldsymbol{x},\boldsymbol{y},t-\tau) \frac{\partial u_{\beta}^{1}}{\partial s}(\boldsymbol{y},\tau) + \right. \\
& \left. + \rho_1 u_{\beta\upsilon}^{1G}(\boldsymbol{x},\boldsymbol{y},t-\tau) \ddot{u}_{\beta}^{1}(\boldsymbol{y},\tau) n_{\delta}^{1}(\boldsymbol{y}) \right\} ds(\boldsymbol{y}) d\tau - \\
& - n_{\gamma}^{1}(\boldsymbol{x}) \int_{0}^{t} \int_{\Gamma_m} \sigma_{\alpha\gamma\beta}^{1G}(\boldsymbol{x},\boldsymbol{y},t-\tau) t_{\beta}^{1}(\boldsymbol{y},\tau) ds(\boldsymbol{y}) d\tau - \qquad \boldsymbol{x} \in \Gamma_C^{+}(t) \qquad (6) \\
& - C_{\alpha\gamma\upsilon\delta}^{1} n_{\gamma}^{1}(\boldsymbol{x}) \int_{0}^{t} \int_{\Gamma_C^{+}(\tau)} \left\{ \boldsymbol{e}_{\varepsilon\delta} \sigma_{\beta\varepsilon\upsilon}^{1G}(\boldsymbol{x},\boldsymbol{y},t-\tau) \frac{\partial \Delta u_{\beta}}{\partial s}(\boldsymbol{y},\tau) + \right. \\
& \left. + \rho_1 u_{\beta\upsilon}^{1G}(\boldsymbol{x},\boldsymbol{y},t-\tau) \Delta \ddot{u}_{\beta}(\boldsymbol{y},\tau) n_{\delta}^{1}(\boldsymbol{y}) \right\} ds(\boldsymbol{y}) d\tau \ ,
\end{aligned}
$$

$$
\begin{aligned}
c_{\alpha\beta}(\boldsymbol{x}) u_{\beta}^{1}(\boldsymbol{x},t) = {} & \int_{0}^{t} \int_{\Gamma_m} \left\{ u_{\beta\alpha}^{1G}(\boldsymbol{x},\boldsymbol{y},t-\tau) t_{\beta}^{1}(\boldsymbol{y},\tau) - \right. \\
& \left. - \sigma_{\beta\gamma\alpha}^{1G}(\boldsymbol{x},\boldsymbol{y},t-\tau) n_{\gamma}^{1}(\boldsymbol{y}) u_{\beta}^{1}(\boldsymbol{y},\tau) \right\} ds(\boldsymbol{y}) d\tau + \qquad \boldsymbol{x} \in \Gamma_m + \Gamma_s \qquad (7) \\
& + \int_{0}^{t} \int_{\Gamma_C^{+}(\tau)} \sigma_{\beta\gamma\alpha}^{1G}(\boldsymbol{x},\boldsymbol{y},t-\tau) n_{\gamma}^{1}(\boldsymbol{y}) \Delta u_{\beta}(\boldsymbol{y},\tau) ds(\boldsymbol{y}) d\tau \ ,
\end{aligned}
$$

$$
c_{\alpha\beta}(\boldsymbol{x}) u_{\beta}^{2}(\boldsymbol{x},t) = \int_{0}^{t} \int_{\Gamma_i} \left\{ u_{\beta\alpha}^{2G}(\boldsymbol{x},\boldsymbol{y},t-\tau) t_{\beta}^{2}(\boldsymbol{y},\tau) - \sigma_{\beta\gamma\alpha}^{2G}(\boldsymbol{x},\boldsymbol{y},t-\tau) n_{\gamma}^{2}(\boldsymbol{y}) u_{\beta}^{2}(\boldsymbol{y},\tau) \right\} ds(\boldsymbol{y}) d\tau, \ \boldsymbol{x} \in \Gamma_i \qquad (8)
$$

where $C_{\alpha\beta\gamma\delta}$ is the elasticity matrix; the quantities with the superscript *G* are 2-D elastodynamic Green's functions for stresses or displacements [8]; $\Delta u_{\beta}(\boldsymbol{y},t)$ is the crack opening displacements (CODs) defined as $\Delta u_{\beta}(\boldsymbol{y},\tau) = u_{\beta}(\boldsymbol{y} \in \Gamma_C^{+},\tau) - u_{\beta}(\boldsymbol{y} \in \Gamma_C^{-},\tau)$; and $c_{\alpha\beta}(\boldsymbol{x})$ is a constant matrix which depends on the position of the collocation point $\boldsymbol{x}$ and reduces to $\delta_{\alpha\beta}/2$ for a smooth boundary (where $\delta_{\alpha\beta}$ is Kronecker delta). All integrals are in the sense of Cauchy principal value. The tensor $\boldsymbol{e}_{\varepsilon\delta}$ is the 2-D permutation tensor [8].

In the current application, the system of equations (6)-(8) has been converted into a 'discrete' form by using discretization in both time and space with proper interpolation functions. The time interval of interest $[0, t]$ is equally divided into m time steps of span Δt. Space-constant boundary elements are employed to divide all of the external boundaries (including the interface) of matrix and inclusion. Straight boundary elements of constant length Δy_C are chosen to discretize the crack face. The unknown CODs, displacements and tractions along the boundaries are approximated by using the interpolation functions in both time and space with the same shapes as those adopted in [6,8]. It is particularly mentioned that special "crack-tip elements" are applied behind crack-tips while constant elements are used away from crack-tips [6,8]. Then the system of equations (6)-(8) in conjunction with the boundary conditions (1)-(4) can be rewritten into a set of algebraic equations for the unknown coefficients, which can be solved using a Gaussian elimination scheme. The crack propagation is simulated by adding a new element on the growing crack tip at an adaptable time which is determined by a dynamic fracture criterion. The fracture criterion used here is similar to the maximum circumferential stress criterion developed by Erdogan and Sih [9], which states that crack advance will take place in the direction θ_0 of the maximum circumferential stress $\sigma_{\theta\theta}$ when this stress reaches the same critical value as in pure mode I fracture. But here $\sigma_{\theta\theta}$ and dynamic fracture toughness K_{ID} are the functions of the crack-tip speed.

4 NUMERICAL RESULTS AND DISCUSSION

As a simple example, we consider the dynamic interaction between a propagating edged crack and a circular inclusion embedded in a square plate under the concentrated impact load $F_0 H(t)$, see Fig.2. The geometry parameters of the system are listed: side length of the square plate 2W=40mm, inclusion radius *r*=4mm and initial crack length a_0=15mm. Some material constants are fixed as $\nu_1 = \nu_2$=0.3 and $\rho_1 = \rho_2 = 5000\mathrm{kg\cdot m^{-3}}$. Without special explanations, crack offset *d*=4mm; the fracture toughness of the plate K_{IC}=49.5× $10^6\,\mathrm{Pa\cdot m^{1/2}}$; and the dynamic fracture toughness K_{ID} as a function of the crack tip velocity *v* is computed by an empirical formula [8]

$$K_{\mathrm{ID}} = K_{\mathrm{IC}} \times \left[1.0 + 2.5 \times (v / C_T^1)^2 + 3.9 \times 10^4 \times (v / C_T^1)^{10}\right]. \tag{9}$$

In calculation, the crack is divided into 24 elements. The concentrated load is distributed over the first element in the left.

The effect of the shear modulus ratio $\mu_{12} = \mu_1 / \mu_2$ on the crack trajectory is shown in Fig.3. It is seen that the crack deflects near to the softer inclusion (μ_{12}=2.0) and away from the stiffer one (μ_{12}=0.5). The crack advances along a straight path for μ_{12}=1.0 since the system becomes a homogeneous plate in this case.

Fig.4a and 4b present the history of the first (K_{I}) and second (K_{II}) dynamic stress intensity factors (DSIFs) for some selected values of μ_{12}, where the DSIFs are non-dimensionalized by $K_0 = \sigma_0 (\pi a)^{-1/2}$ with $\sigma_0 = F_0 / \Delta y_C$. We find the values of K_{II} oscillate near zero and those of K_{I} oscillate and ascend to a high level. This implies that the propagating crack is in mode I. It is noted that the value of K_{I} is negative in some time period. This means that the crack closure takes place. This behavior, we believe, is due to the far distance of the crack tip from the load. The interaction between the crack faces should be considered in more precise analysis. But here we neglect this effect.

The crack arc length and crack tip speed are plotted in Fig.5a and 5b for different values of μ_{12}.

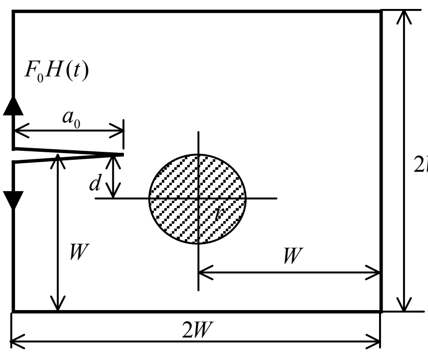

Fig.2 A propagating edged crack and a circular inclusion in a square plate

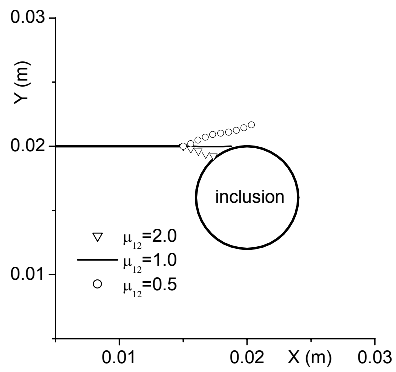

Fig.3 Effects of the shear modulus ratio on crack trajectory

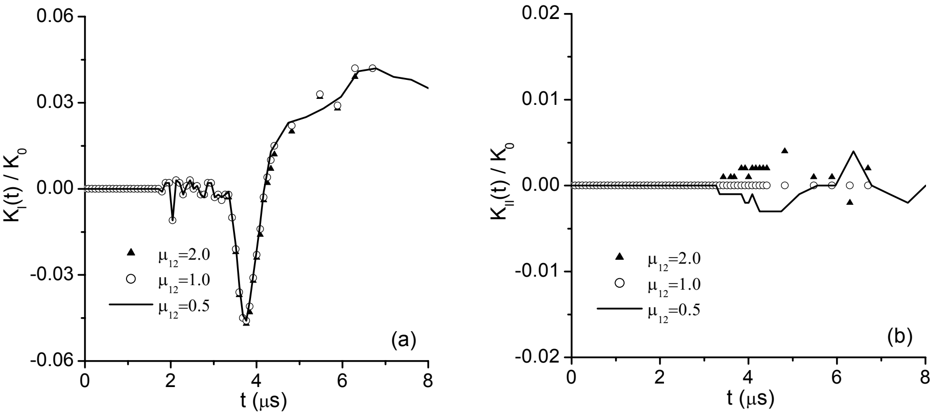

Fig.4 Effects of the shear modulus ratio on DSIF, K_I (a) and K_{II} (b)

The crack initiation time has a slight difference and the earlier crack initiation appears for the stiffer inclusion. It is noted that arrest appears temporarily for a very short time period during the crack propagation for μ_{12}=2.0 and 1.0. This sounds very strange.

Next we consider the effect of the dynamic fracture toughness on the crack propagation, see Fig.6a where we choose $\mu_{12} = 0.5$. Three cases are considered: (*i*) K_{IC}=49.5× $10^6\,\mathrm{Pa \cdot m^{1/2}}$; (*ii*) K_{IC}=7.60× $10^6\,\mathrm{Pa \cdot m^{1/2}}$; and (*iii*) $K_{ID} = K_{IC}$=49.5× $10^6\,\mathrm{Pa \cdot m^{1/2}}$ (i.e. K_{ID} is independent of the crack speed). It can be found that the crack deflects farther for case (*iii*) than for cases (*i*) and (*ii*). The effect of the inclusion location (d/r) on the crack trajectory is demonstrated in Fig.6b for μ_{12}=0.5. The kink angle of the crack is larger for the smaller value of d/r.

ACKNOWLEDGEMENTS

Support by the China National Natural Science Foundation under Grant No. 10025211 is gratefully acknowledged.

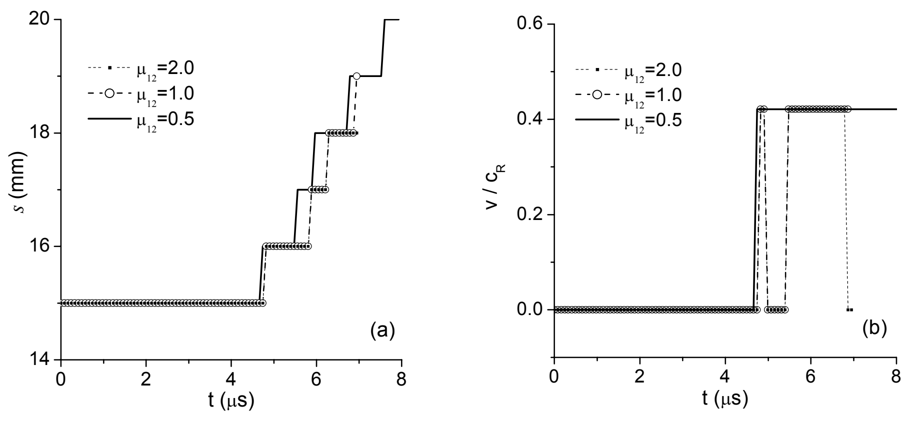

Fig.5 Effects of the shear modulus ratio on crack length (a) and speed (b)

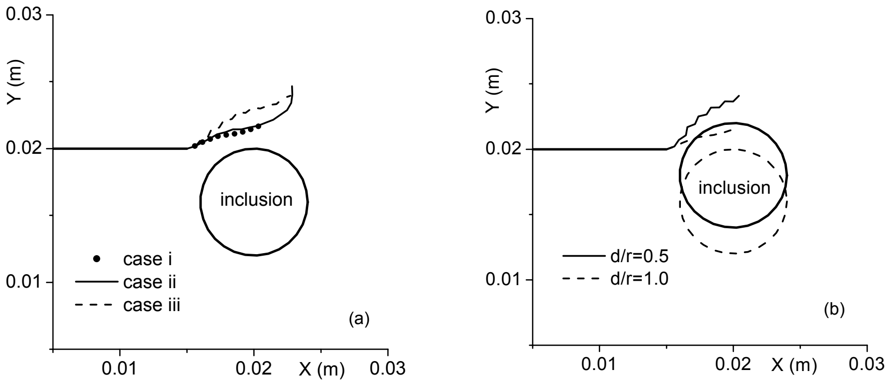

Fig.6 Effects of the fracture toughness (a) and inclusion position (b) on crack trajectory

REFERENCES

[1] Erdogan, F., Gupta, G. D. and Ratwani, M. Interaction between a circular inclusion and an arbitrarily oriented crack. *Journal of Applied Mechanics* **41**(1974), 1007–1013.

[2] Erdogan, F. and Gupta, G. D. The inclusion problem with a crack crossing the boundary. *International Journal of Fracture* **11**(1975), 13–27.

[3] Kassam, Z. H. A., Zhang, R. J. and Wang, Z. Finite element simulation to investigate interaction between crack and particulate reinforcements in metal-matrix composites. *Materials Science and Engineering* **A203**(1995), 286–299.

[4] Bush, M. B. The interaction between a crack and a particle cluster. *International Journal of Fracture* **88**(1997), 215–232.

[5] Knight, M. G., Wrobel, L. C., Henshall, J. L. and Lacerda, L. A. A study of the interaction between a propagating crack and an uncoated/coated elastic inclusion using BE technique. *International Journal of Fracture* **114**(2002), 47–61.

[6] Lei, J., Wang, Y. S. and Gross D. Dynamic interaction between a sub-interface crack and the interface in a bi-material: time-domain BEM analysis. *Archive of Applied Mechanics* **73**(2003), 225-240.

[7] Zhang, Ch. and Gross, D. A non-hypersingular time-domain BIEM for transient elastodynamic crack analysis. *International Journal of Numerical Methods in Engineering.* **36**(1993), 2997-3017.

[8] Seelig, Th. *Zur Simulation der Dynamischen Rißausbreitung mit einer Zeibereichs- Randlementmethode*. Dissertation, TU-Darmstadt, Germany, 1997.

[9] Erdogan F. and Sih G. C. On the crack extension in plates under plane loading and transverse shear. *Journal of Basic Engineering* **85**D(1963), 519-525.